

# Evanescent Wave-based Near-wall Thermometry Utilizing Brownian Motion

Kanjirakat Anoop

Micro Scale Thermo Fluids (MSTF) Laboratory  
Texas A&M University at Qatar  
Doha, Qatar  
e-mail: anoop.baby@qatar.tamu.edu

Reza Sadr

Micro Scale Thermo Fluids (MSTF) Laboratory  
Texas A&M University at Qatar  
Doha, Qatar  
e-mail: reza.sadr@qatar.tamu.edu

**Abstract**—Evanescent wave-based Particle Image Velocimetry (or nPIV) is known to be an effective tool in estimating near-wall velocity fields. nPIV uses evanescent wave illumination of particle tracers in the fluid within order of  $O(100\text{nm})$  from the wall where illumination intensity decays exponentially with distance normal to the wall. Brownian motion of the sub-micron tracer particles used in nPIV is a function of fluid temperature in this region. Monte Carlo simulation of particle movement in this region is used to investigate the possibilities of utilizing this effect for near-wall thermometry. Synthetic nPIV images of the illuminated polystyrene particles of 100nm diameter in the near-wall region are initially generated for different fluid temperature measurement. The spatial distribution of the particles takes into account the forces such as buoyancy, electrostatic repulsion and van der Waals attraction, in addition to the hindered Brownian motion near the walls. The synthetic images were then processed using standard cross-correlation function. The results of the numerical simulation show that the temperature variation causes a change in width and height of the nPIV correlation function. Initial experimental studies are conducted to verify the results of simulations.

**Keywords**—Total Internal Reflection; nPIT; thermometry.

## I. INTRODUCTION

Near-wall temperature measurement of a fluid at micro scale is an important part of studying convection heat transfer. Nano/micro-fabricated thermocouples and resistance temperature detectors (RTD) provides the highest out-of-plane resolution for temperature measurement [1]. However, these sensors are often complicated, somehow intrusive and can affect the flow structure in micro-scale flows. Non-intrusive thermometry such as infrared thermometry (IRT), molecular tagging thermometry (MTT), laser induced fluorescence thermometry (LIFT) and particle image velocimetry (PIV) based thermometry are generally preferred for micro-scale flow investigations [2]. In micro/nano-PIV, fluorescent tracer particles are seeded in the fluid to track the flow assuming they faithfully follow the fluid. Inevitably, as the seeding particle sizes are small, they undergo Brownian motion, where at low speed; this could introduce undesirable bias in the velocity measurements. The effect of the Brownian motion in PIV when using cross-correlation method, is a width-wise spreading of correlation peak. This effect is generally undesirable in velocimetry as it

reduces signal-to-noise ratio of the results and increases the uncertainty in determination of the averaged particle displacement. Olsen and Adrian [3] proposed that such spreading of correlation peak could be utilized for thermometry, as Brownian motion of the seeded particles has direct dependence on temperature. Hohreiter et al. [4] demonstrated the use of correlation based micro-PIV technique utilizing Brownian motion of seeded particles to determine temperature. Their result shows a temperature measurement with an experimental accuracy of  $\pm 3^\circ\text{C}$  inside a micro channel. In a separate study, Chamarthy et al. [5] noted that low image density PIV tracking method to process particle images performed better than cross-correlation based thermometry. The average difference between the predicted and measured fluid temperature was recorded to be  $\pm 2.6^\circ\text{C}$  at an out-of plane resolution of  $\sim 20\mu\text{m}$ .

Zettner and Yoda [6] introduced an extension to  $\mu\text{PIV}$  technique based on evanescent-wave illumination generated by total internal reflection (TIR) of a laser beam at the fluid-solid interface between the flow and the wall, known as nano-PIV (nPIV). Sadr et al. [7] investigated the introduced error in velocity measurements as a result of particle mismatch due to “drop out” and “drop in” of particle tracers in the illuminated region brought in by the effects of hindered Brownian motion. Later, using an analytical approach, Sadr et al. [8] introduced an empirical relation between mean particle displacement and the average shear fluid velocity in the near-wall region with a given thickness. This was later expanded by studying the effects of Brownian motion, light penetration profiles, surface forces such as van der Waals, and electrostatic forces and the velocity gradient on the near-wall measurements using a traditional PIV cross-correlation method [9].

This paper extends the applicability of nPIV technique for temperature measurements utilizing the Brownian motion of seeded particles and proposes the use of nPIT (nano-particle image thermometry) technique for investigating near-wall temperatures. Monte Carlo simulation [8] is used to generate artificial images of particles in the evanescent wave region. Simulations are performed for fluid at stationary condition at different temperatures to simulate Brownian motion at varying temperatures. Effect of non-uniform illumination, hindered Brownian motion and the surface forces acting on the particles near the wall are considered while generating images of particles. Image pairs generated with a given time delay are cross-correlated to

analyze the spread of correlation peak width with temperature. Details of the methodology and theoretical model used are discussed next. Finally, experimental efforts are reported to verify the results of the simulations.

## II. THEORETICAL MODEL

As mentioned earlier, in nPIV evanescent wave generated at the glass water interface is used to illuminate particles only in the near-wall region. When a light beam travels through a medium, with a refractive index  $n_1$ , into another transparent medium with a lower refractive index of  $n_2$  at an angle exceeding the critical angle,  $\theta_c = \sin^{-1}(n_2/n_1)$ , it is totally reflected at the interface. However, the electromagnetic field penetrates into the lower refractive index region and propagates for a small distance parallel to the interface creating what is called an evanescent wave. This evanescent wave is capable of exciting fluorescent particles in this region while the large numbers of particles farther away in the bulk liquid remain unexcited. Evanescent wave intensity,  $I$ , in the direction normal to the interface decays exponentially with distance,  $z$ :

$$I = I_0 \exp(-z/z_p) \quad (1)$$

where  $I_0$  is the maximum intensity at the wall and  $z_p$  is the penetration depth:

$$z_p = \frac{\lambda_0}{4\pi n_1} \left[ \sin^2 \theta - \left( \frac{n_2}{n_1} \right)^2 \right]^{-\frac{1}{2}} \quad (2)$$

$\lambda_0$  is the wavelength of the light and  $\theta$  is the incident angle. For visible light at a glass water interface,  $z_p$  is on the order of O(100nm). Figure 1 shows the schematic of a general TIRF setup used in an nPIV experiment where only the near-wall fluorescent particles in the fluid are excited and viewed from the bottom of the microscope plate. The emission intensity of the tracer particles in this region is also an exponential function of the distance from the wall with a decaying trend as stated by Equation 1. However, depending on the optical characteristics of the imaging system, ultimate depth of visible region,  $z_v$ , depends on the intensity of the incident laser beam, fluorescent particle characteristics, camera and the background noise of the imaging system. In practice, this depth is usually more than the estimated penetration depth. In nPIV the focal depth of the objective lens is larger than the penetration depth of the evanescent wave, therefore, all the particles in the image are in focus and there is no back-ground light.

For a stationary fluid, the particle movement is a result of Brownian motion and surface forces. Brownian motion is the micro-scale movement of particles immersed in a fluid as a result of the thermal energy of the fluid. At submicron scale, Brownian displacement is of the same length scale as that of fluid convection and therefore becomes important during fluid velocimetry. Brownian motion is usually expressed in terms of its diffusion coefficient.

In an unconfined flow, Brownian diffusion coefficient is represented in the form of the Stokes-Einstein equation [10]:

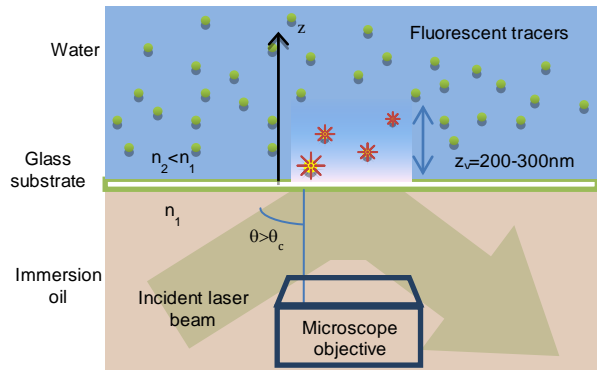


Figure 1. Schematic of nPIV measurement technique.

$$D = \frac{kT}{6\pi\mu a} \quad (3)$$

where  $k$  is the Boltzmann constant,  $T$  and  $\mu$  are temperature and viscosity of the fluid, respectively. For liquids, with increase in temperature, absolute viscosity value decreases. Hence, for a smaller seeding particle diameter (100nm in this case) diffusion coefficient increases with increase in temperature when suspended in a liquid. Quantifying the relative change in random particle movement due to Brownian motion is the key principle used in nPIT.

In the near-wall region, where nPIT is interrogating, the diffusion coefficient is hindered due to the additional hydrodynamic effects at the wall and the Brownian diffusion coefficient,  $\beta$ , can be expressed in the tensor form as:

$$D = \begin{bmatrix} D_x & 0 & 0 \\ 0 & D_y & 0 \\ 0 & 0 & D_z \end{bmatrix} = D \begin{bmatrix} \beta_{\parallel} & 0 & 0 \\ 0 & \beta_{\parallel} & 0 \\ 0 & 0 & \beta_{\perp} \end{bmatrix} \quad (4)$$

where  $\beta_{\perp}$  and  $\beta_{\parallel}$  are the wall correction factors for movement perpendicular and parallel to the wall, respectively [11]:

$$\beta_{\parallel} = \left[ 1 - \frac{9}{16} \left( \frac{a}{z} \right) + \frac{1}{8} \left( \frac{a}{z} \right)^3 - \frac{45}{256} \left( \frac{a}{z} \right)^4 - \frac{1}{16} \left( \frac{a}{z} \right)^5 \right], \quad (5)$$

and

$$\beta_{\perp} = \left[ \frac{2h \cdot (3h + a)}{(6h^2 + 9ah + 2a^2)} \right] \quad (6)$$

where  $a$  is the particle radius and  $h = (z - a)$ . As the particles move away from the wall, the correction factors tend to unity and the diffusion coefficient tends to that of the Stokes-Einstein value. In present simulation, this anisotropic nature of Brownian diffusion coefficient is considered.

Particle displacements due to Brownian motion are obtained from Langevin equation, which describes the displacement of a spherical particle,  $\Delta \vec{x}$ , over a time period,

$\Delta t$ , [12]. For a stationary fluid with no external forces acting on the particle, the Langevin equation in  $x$  direction reduces to [11]:

$$\Delta x = \sum_{t=0}^{t=\Delta t} \{ \chi \delta r_x \} \quad (7)$$

where  $\chi$  is an array of normally distributed random numbers with a mean of zero and a standard deviation of one and  $\delta r = \sqrt{2D\delta t}$ . In  $z$  direction, perpendicular to the wall, there is no translational velocity and only the first term in the Langevin equation reduces to:

$$\Delta z = \sum_{t=0}^{t=\Delta t} \left\{ \frac{D_z}{kT} F_z \delta t + \frac{dD_z}{dz} \delta t + \chi \delta r_z \right\} \quad (8)$$

External forces acting on particles in the direction perpendicular to the wall include, electrostatic forces and van der Waals forces [13, 14],  $F_{el}$  and  $F_{vdw}$ , respectively, caused by the presence of the wall, plus buoyancy force,  $F_b$ , which is a result of density mismatch between the suspending medium and the tracer particles. The total force acting on a particle in the direction normal to the wall would be the summation of all these forces,  $F_z = F_{el} + F_{vdw} + F_b$ , where, the combined effects of electrostatic, van der Waals, and buoyancy forces generate a net repulsive force that pushes the tracers away from the wall [9].

### III. MONTE CARLO SIMULATION

Simulations are carried out with exponentially decaying illumination. Artificial images of tracer particles at time  $t = 0$  and later at time  $t = \Delta t$  are generated. Particle displacements in the  $x$ ,  $y$  and  $z$  directions are calculated for different time steps of  $\Delta t = \sum \delta t$  using equations 7 and 8 which encompasses the effects of Brownian motion and other external forces. The time step  $\delta t = 5 \mu s$  used in this work is much smaller than  $\Delta t$  and is an order of magnitude larger than the particle momentum relaxation time. Particle-wall collisions are considered to be perfectly elastic, preventing any particles from going 'through' the wall.

Non-uniform illumination is considered while generating artificial images for present work replicating an actual evanescent wave illumination. The brightness (size) of the particle images are a function of their distance from the wall, where particles near the wall look bigger and brighter than those further away. By implementing an exponentially decaying intensity of illumination normal to the wall, variation in particle image sizes in the field was created. Particle images in this work were assumed to be circular with a Gaussian intensity distribution profile with a peak grayscale value calculated using the equation

$$I_p = C \cdot \exp(-h / z_p) \quad (9)$$

where  $h = (z - a)$  and  $C$  represents the net power emitted and collected from the bottom of each sphere and  $a$  is particle radius [7]. The effective particle image diameter,  $D_{\text{image}} = 8$  pixels, has an Airy disk pattern, which can be

approximated using a Gaussian profile with an approximate diameter of the point spread function of the microscope system [15]. Electronic noise and shot noise are also added to the image using a combination of white and Gaussian distribution noise, respectively [9] to mimic real image characteristics.

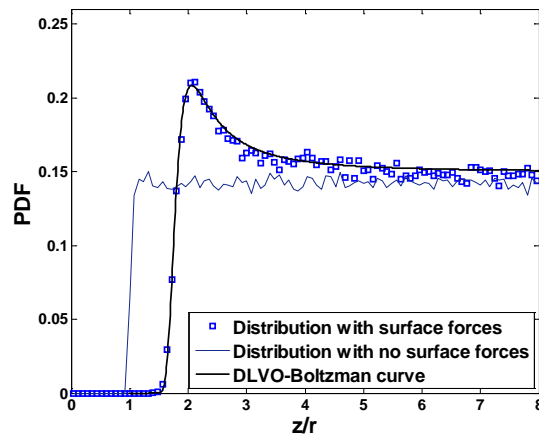


Figure 2. PDFs of particle distribution throughout  $z_v$ .

Initially, 1500 particles of radius 50 nm are distributed over a distance of  $5z_p$  normal to the wall in the fluid for simulation. This results in a particle density of  $\sim 1.89$  particles/ $\mu m^3$ , in an image size of (653x70) pixels in the  $x$  and  $y$  directions, similar to actual experimental images. Particles are initially uniformly distributed in the flow and then surface forces move the particles to their final steady state distribution. The final Probability Distribution Function (PDF) of the particles throughout the visible region,  $z_v$ , at this stage is shown in Fig. 2 for two cases of a) no surface forces, b) surface forces for  $\zeta$ -potentials of  $\zeta_{\text{particle}} = 100\text{mV}$  and  $\zeta_{\text{wall}} = 80\text{mV}$  respectively [16, 17]. The surface forces and zeta potential of the particles and surface contribute significant effect in the distribution of particles near the wall. As can be seen from the figure, when the surface forces effects are considered, the particles are seen pushed away from the wall region, making sparse density of particles near to the walls. It is also observed that the steady state probability distribution function of the particles, for a given surface force, can adequately be modeled by a Boltzmann profile as reported before [16]. In present simulations, inter-frame time delays more than 2ms are used. This is mainly due to the fact that longer time delays provided better measurement sensitivity with variation in temperature. However with increase in time delays, the noise-to-signal ratio also increased, reducing the accuracy.

### IV. RESULTS AND DISCUSSION

2500 independent artificial image pairs of 653 x70 pixels of tracer particles at time  $t=0$  and later at time  $t=\Delta t$  were generated. The images in each pair were then post-processed using a standard FFT-based cross correlation program that uses a 3D Gaussian peak finding algorithm based on a Gaussian surface fit [9]. Each image was divided into five adjacent interrogation windows, each 186x68 pixels size

with an overlap of ~50%, with the midpoints positioned along the center line of the image in the  $y$  direction. The image pairs are then cross-correlated to obtain the cross correlation coefficient.

Figure 3 shows the cross-correlation coefficient variation for different fluid temperatures after ensemble averaging. As can be noted, the peak height decreases whereas the peak width of the correlation increases with increase in fluid temperature. The above variation is for an inter-frame time delay of 3ms. The correlation function as depicted in Fig. 3 is obtained after carrying out ensemble averaging of all the correlation planes of 2500 image pairs. The main advantage of ensemble averaged correlation approach is the fact that the noise in individual correlation planes is significantly reduced by having an averaged correlation plane.

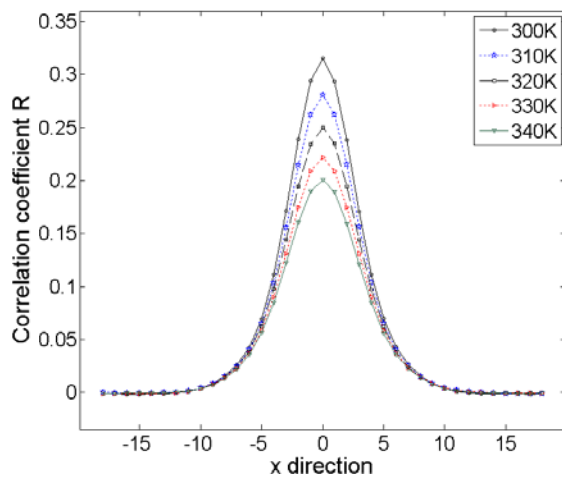


Figure 3. Cross-correlation coefficient for different fluid temperatures

Usually, ensemble averaging alone would mitigate the noises present, however, it is noticed in the simulations that there exists some correlation planes (about 1-2%) which had higher noise-to-signal ratio. Including them in analysis, would increase the uncertainties while determining peak widths and heights. Hence, before averaging bad correlation planes that are having a noise-to-signal ratio below 0.9 are removed from the analysis. It is noted that at lower temperatures, more number of correlation planes exists which has lower noise-to-signal ratio. As temperature is increased, the number of correlations with higher noise-to-signal ratio also increased. Since correlations with lower noise-to-signal ratio could adversely affect the peak width and height evaluation.

Figure 4(a) shows peak width variation with temperature for two inter-frame time delays of 3ms and 5ms. Peak width is estimated by fitting a Gaussian surface with at least 13 points in the peak region:

$$G(x, y) = A \cdot e^{-\frac{(x-x_0)^2}{2\sigma_x^2}} \times e^{-\frac{(y-y_0)^2}{2\sigma_y^2}} \quad (10)$$

where  $A$  is the peak height and  $\sigma_x$  and  $\sigma_y$  are representatives peak widths in  $x$  and  $y$  directions.

For a stationary fluid, both the widths should be similar in magnitude [5]. The error bars as depicted in the figure represent 95% confidence levels of the presented data calculated as suggested by Benedict *et al.* [18]. A close observation of the figure shows that the uncertainty in the width estimated for a time delay of 5ms is higher than that for 3ms. Uncertainties are also observed to be higher at the higher temperatures. The reason for the above observation would be an existence of a better correlation, which is having a smaller spread in uncertainties at lower time delays. However, higher temperature sensitivity is observed for the longer time delays, as the effect of temperature on Brownian motion is more reflected when time delays are higher.

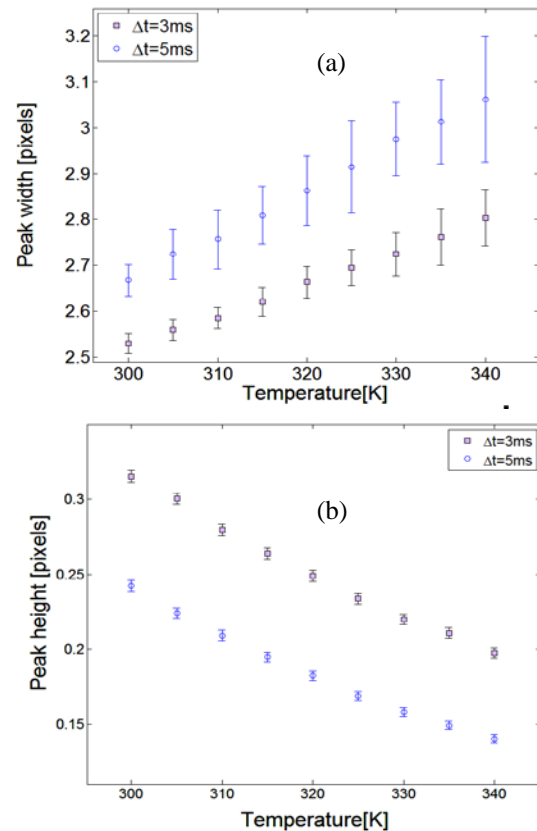


Figure 4. (a) Peak width variation with temperature (b) Peak height variation with temperature.

Figure 4(b) shows variation of the peak height with temperature for the same time delays as given in Fig. 4(a). As peak width and height variations seem to have opposing trends, therefore, the ratio of peak width to height would be a better parameter for thermometry. Peak width to height ratio variation for various temperatures for two time delays is depicted in Fig. 5. In this figure also, the sensitivity with temperature is seen to be more for 5ms than for 3ms. However, the uncertainties are lower in the case when the inter-frame time delay was 3ms. It can be concluded that the ratio of correlation width to height may be used to obtain fluid temperature in the near-wall region for an nPIT setup. After noticing the feasibility of using nPIT technique based on synthetic images efforts are made to conduct experiments.

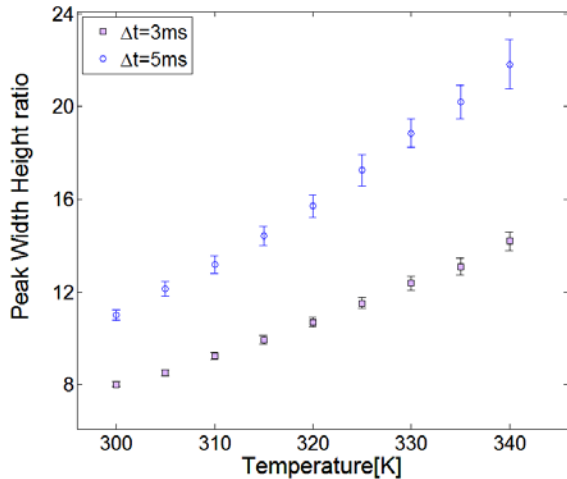


Figure 5. Variation of peak width to height ratio with temperature

### V. INITIAL EXPERIMENTS

Some initial experiments are conducted to practically validate the observed effects of simulations. An experimental setup as depicted in Fig. 6(a) is used to confine the fluid at a constant temperature and to analyze the Brownian motion of seeded particles. Constant temperature condition is achieved using a temperature controlled microscope stage. The temperature of the stage is adjusted by circulating water from a constant temperature water supply (F25-ED Julabo). A metal substrate with a hole drilled and a glass coverslip (0.13mm thick) pasted below holds the sample fluid. The heat from the microscope stage is effectively conducted to the sample fluid through the metal substrate. The fluid temperature is recorded using a precision K-type thermocouple inserted in the sample through an insulated block, placed on top of the metal substrate.

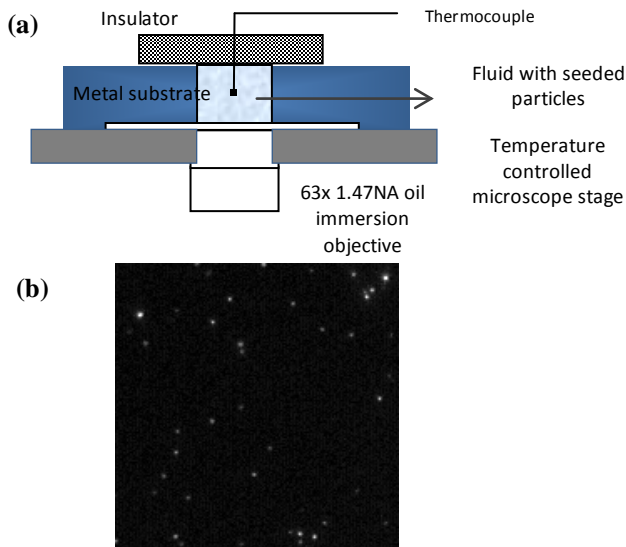


Figure 6. (a) Schematic of experimental setup used (b) Typical nPIV image obtained

An Argon-Ion CW laser beam with a wave length of 488 nm (Spectra Physics BeamLok 2060) was used to provide excitation light in the near-wall region. Images were obtained using an EMCCD camera (ProEM 512, Princeton Instruments) attached to an inverted epi-fluorescence microscope (Leica DMI6000B) via a 63x 1.47NA oil immersion objective. The pixel resolution for the images obtained from this imaging set up was  $4 \times 10^6$  (pixel/meter). The nPIV seeding particles used were 100nm ( $\pm 5\%$ ) diameter polystyrene fluorescent particles (F8803, Invitrogen) having peak excitation and emission wavelengths of 505nm and 515nm, respectively. In all the experimental runs, the fluorescent particle concentration was maintained at a constant volume concentration of 0.017%. Evanescent wave illumination was generated on the bottom glass-water interface in the microchannel. The angle of incidence of light in the water-quartz interface was evaluated to be  $75^\circ$ , based on the numerical aperture value of the objective lens and refractive indices at the interface. This yielded a penetration depth of  $z_p \cong 105\text{nm}$  (Eq. 2). The depth of visible region ( $z_v$ ) is then estimated to be 310nm for the basefluid. This estimation is based on the penetration depth and the intensity value of the background noise in captured images. A typical nPIT image obtained during experimentation is shown in Fig. 6 (b).

For each experiment, 1500 nPIT image pairs of 200x200 pixels were acquired with a inter frame time delay of 0.5 ms. The interrogation window size was set at 186x68 pixels with a search radius of 15 pixels. In each case, there were sufficient numbers of matched tracer particles in the interrogation windows. The images are then post-processed using the same cross-correlation program used in the simulation section to determine the correlation peak width and height.

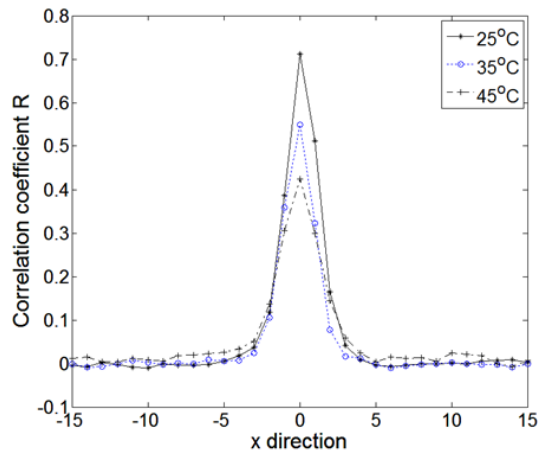


Figure 7. Experimental cross-correlation coefficient for different fluid temperatures

Figure 7 shows the experimental observation of cross-correlation function for temperatures varied from 25°C to 45°C. The trend of peak height reduction and peak width

broadening are observed to be similar to that of the simulations. In order to strengthen the correlation and to reduce the spread of uncertainties in peak width, a smaller inter-frame time delay of 0.5ms is considered in the experiment. However, experimental uncertainties are observed to be much higher than simulations. Nevertheless, the initial experimental results are presently reported here to show the practical feasibility of using nPIT technique and more strenuous efforts are required in future to obtain a highly repeatable cross-correlation relation with temperature.

## VI. CONCLUSIONS AND FUTURE WORK

The present work investigated the feasibility of using evanescent wave illumination technique for temperature measurement. Monte Carlo simulation is used to artificially generate nPIV images of stationary fluid seeded with fluorescent particles with an exponentially decaying intensity from the wall. These images are then cross-correlated to investigate the effect of temperature on the peak width and height of the cross-correlation function. The results of simulations show that correlation width increase whereas its height decreases with increase in fluid temperature. Uncertainties in the measured peak width are lower when the inter-frame time delays are short. However, the sensitivity with temperature is observed to be more when the time delays are longer. Peak width to height ratio is observed to be a better parameter for quantifying while using nPIT technique. More elaborate experimental observations with varying time delays are required in the future in order to completely quantify the effect of Brownian motion on thermometry.

## ACKNOWLEDGMENT

This publication was made possible by NPRP grant # 08-574-2-239 from the Qatar National Research Fund (a member of Qatar Foundation). The statements made herein are solely the responsibility of the authors.

## REFERENCES

- [1] P. R. N. Childs, J. R. Greenwood, and C. A. Long, "Review of temperature," *Review of Scientific Instruments*, vol. 71, pp. 2959-2978, 2000.
- [2] P. Chamarthy, S. V. Garimella, and S. T. Wereley, "Measurement of the temperature non-uniformity in a microchannel heat sink using microscale laser-induced fluorescence," *International Journal of Heat and Mass Transfer*, vol. 53, pp. 3275-3283, 2010.
- [3] M. G. Olsen and R. J. Adrian 2000, "Brownian motion and correlation in particle image velocimetry," *Optics & Laser Technology* vol. 32, pp. 621-627, 2000.
- [4] V. Hohreiter, S. T. Wereley, M. G. Olsen, and J. N. Chung, "Cross-correlation analysis for temperature measurement," *Measurement Science and Technology*, vol. 13, pp. 1072-1078, 2002.
- [5] P. Chamarthy, S. V. Garimella, and S. T. Wereley, "Non-intrusive temperature measurement using microscale visualization techniques," *Experiments in Fluids*, vol. 47, pp. 159-170, 2009.
- [6] C. M. Zettner and M. Yoda, "Particle velocity field measurements in a near-wall flow using evanescent wave illumination," *Experiments in Fluids*, vol. 34, pp. 115-121, 2003.
- [7] R. Sadr, H. Li, and M. Yoda, "Impact of hindered brownian diffusion on the accuracy of particle-image velocimetry using evanescent-wave illumination," *Experiments in Fluids*, vol. 38, pp. 90-98, 2005.
- [8] R. Sadr, C. Hohenegger, H. Li, P. J. Mucha, and M. Yoda, "Diffusion-induced bias in near-wall velocimetry," *Journal of Fluid Mechanics*, vol. 57, pp. 443-56, 2007.
- [9] R. Sadr, K. Anoop, and R. Khader, "Effects of surface forces and non-uniform out-of plane illumination on the accuracy of nPIV velocimetry," *Measurement Science and Technology*, vol. 23, 055303, 2012.
- [10] A. Einstein, "Uber die von der molekularkinetischen theorie der warme geforderte bewegung von in ruhenden flussigkeiten suspendierten teilchen," *Ann Physics*, vol. 17 pp. 549, 1905.
- [11] M. A. Bevan and D. C. Prieve, "Hindered diffusion of colloidal particles very near to a wall: revisited," *Journal of Chemical Physics*, vol. 113, pp. 1228-36, 2000.
- [12] A. T. Clark, M. Lal, and G. M. Watson, "Dynamics of colloidal particles in the vicinity of an interacting surface," *Faraday Discussion of the Chemical Society*, vol. 83 pp. 179-191, 1987.
- [13] M. Oberholzer, N. Wagner, and A. M. Lenhoff, "Grand canonical Brownian dynamics simulation of colloidal adsorption," *Journal of Chemical Physics*, vol. 107 9157-67, 1997.
- [14] A. Banerjee and K. D. Kihm, "Experimental verification of near-wall hindered diffusion for the Brownian motion of nanoparticles using evanescent wave microscopy," *Physics Review E*, vol. 72, 042101/1-4, 2005.
- [15] C. Meinhart and S. T. Wereley, "The theory of diffraction-limited resolution in microparticle image velocimetry," *Institute of Physics Publishing, Measurement Science and Technology*, vol. 14, pp. 1047-53, 2003.
- [16] P. Huang, J. S. Guasto, and K. Breuer, "The effects of hindered mobility and depletion of particles in near-wall shear flows and the implications for nanovelocimetry," *Journal of Fluid Mechanics*, vol. 637, pp. 241-265, 2009.
- [17] J. A. Fagan, P. J. Sides, and D. C. Prieve, "Calculation of ac electric field effects on the average height of a charged colloid: effects of electrophoretic and Brownian motions," *Langmuir*, vol. 19, pp. 6627-32, 2003.
- [18] L. H. Benedict and R. D. Gould, "Towards better uncertainty estimates for turbulence statistics," *Experiments in Fluids*, vol. 22, pp. 129-136, 1997.